A direct approach to one photon interference contributions in the coherent control of photodissociation

Victor S. Batista[a] and Paul Brumer
Chemical Physics Theory Group, Department of Chemistry, and Photonics Research Ontario, University of Toronto, Toronto, Ontario M5S 3H6, Canada

(Received 13 March 2001; accepted 29 March 2001)

Formally exact quantum mechanical expressions for cumulative transition matrix elements $\mu_{jk}(\xi,E)=\Sigma_n\langle j|\mu_\varepsilon|E,\xi,n^-\rangle\langle E,\xi,n^-|\mu_\varepsilon|k\rangle$, central to one photon coherent control scenarios of photodissociation, are derived. The resultant approach bypasses the need for solving the complete state-to-state quantum mechanical reactive scattering problem to obtain control results. These exact expressions are implemented both quantum mechanically and via a semiclassical initial value representation method to investigate coherent control in the generic photodissociation of a triatomic into more than one product. The semiclassical approach is shown to provide an accurate description of bimolecular control in this system. © *2001 American Institute of Physics.*
[DOI: 10.1063/1.1372713]

I. INTRODUCTION

Developing new laser techniques for controlling the quantum dynamics of polyatomic systems is one of the important challenges in modern photochemistry. The most successful of these approaches is coherent control,[1,2] where quantum interference effects are manipulated to alter the dynamics. With coherent control having been demonstrated both computationally and experimentally for simple photodissociation reactions, the challenges ahead range from investigating yield control in complex molecular environments to demonstrating routes to new products in realistic polyatomic reactions.

Progress in coherent control relies heavily on theoretical and computational approaches which allow an understanding of the dominant interference phenomena and provide a means of designing new control scenarios. However, such approaches are currently restricted to small systems, a limitation of modern computational quantum mechanics. The purpose of this paper is to develop an efficient and rigorous semiclassical approach to simulate coherent control scenarios to allow applications to larger molecular systems. We focus on coherent control scenarios involving interference via one photon routes. This includes controlled photodissociation via bichromatic coherent control[3] or weak field pump–dump schemes.[4]

We consider photodissociation from an initial bound state $|i\rangle$ to the final continuum state $|E,\xi,n^-\rangle$. Here, E,ξ,n denote the total energy, arrangement channel and internal quantum numbers of the product state with which the continuum state $|E,\xi,n^-\rangle$ correlates. In coherent control of photodissociation involving one photon routes, the probability of forming a desired product is a sum of terms, some corresponding to the direct photodissociation of a bound state $|k\rangle$ of the form $\mu_{kk}=\Sigma_n\langle k|\mu_\varepsilon|E,\xi,n^-\rangle\langle E,\xi,n^-|\mu_\varepsilon|k\rangle$, and some to terms of the form $\mu_{jk}=\Sigma_n\langle j|\mu_\varepsilon|E,\xi,n^-\rangle \times\langle E,\xi,n^-|\mu_\varepsilon|k\rangle$. The latter correspond to interference between one photon absorption routes to the continuum from level $|j\rangle$ and from level $|k\rangle$. Both of these terms involve a sum over all final states. It therefore appears that obtaining μ_{jk} requires solving the scattering problem at the complete state-to-state level, a task which becomes increasingly difficult as the size of the system increases. In this paper we show that this is not the case, i.e., that a direct method for obtaining these terms, based on a correlation function approach, considerably simplifies this computation.

In particular, in this paper we make two contributions towards the goal of developing useful methods for coherent control computations. First, we develop formally exact quantum expressions for cumulative transition matrix elements that circumvent the need to solve the reactive scattering problem at the complete state-to-state level. Second, we implement this approach semiclassically via the initial value representation (SC-IVR) to examine a specific control scenario, bichromatic control, on a (collinear) polyatomic problem dissociating to two chemically distinct products, and show that the results are in very good agreement with exact quantum computations.

In recent years, there has been a rebirth of interest in the SC-IVR approach, a method originally due to Miller,[5] as a means of including quantum effects in molecular dynamics.[6–21] However, to date, the only SC-IVR application to coherent control is our recent study of bichromatic coherent control of nonadiabatic ICN photodissociation.[22] In that work, the SC-IVR was shown capable of reproducing both amplitudes and *phases* of the μ_{ij} in an approach that required solving the full scattering problem at the asymptotic state-to-state level. The resultant semiclassical photofragmentation ratios were found to be in good agreement with quantum simulations. Here we extend this approach, dealing with a reactive photodissociation problem via the ''direct''

[a]Current address: Department of Chemistry, Yale University, New Haven, Connecticut 06520-8107.

implementation procedure of the SC-IVR for computations of cumulative transition matrix elements.

The paper is organized as follows: In Sec. II, and the Appendix, we review the bichromatic coherent control scenario and derive formally exact expressions for the cumulative transition matrix elements. Sections III and IV describe procedures to implement these expressions in terms of the SC-IVR, and also in terms of exact quantum mechanical methods based on the split-operator propagation scheme.[23] Section V evaluates these expressions for a simple example of unimolecular decomposition, and compares the semiclassical results with full quantum mechanical simulations. The Appendix contains a derivation of an important expression for the projection operator onto fixed total energy and specific product channel. Section VI contains a summary and conclusions.

II. COHERENT CONTROL IN A CONTINUUM STATE

We consider bichromatic coherent control[3] in the unimolecular decomposition reaction of a generic polyatomic molecular system ABC that photodissociates according to

$$ABC+\hbar\omega \begin{array}{l} \overset{(\xi=1)}{\rightarrow} C+AB(n) \\ \overset{(\xi=2)}{\rightarrow} A+BC(n). \end{array} \tag{2.1}$$

Here $\xi=1,2$ denotes the final arrangement and n denotes the internal states of the product.

The molecule ABC is prepared in an initial superposition state,

$$|\Psi_0(j,k)\rangle=|\Phi_g\rangle[c_j|j\rangle+c_k|k\rangle], \tag{2.2}$$

where $|\Phi_g\rangle$ is the ground electronic state wave function, and $|j\rangle$ is the nuclear eigenstate of energy E_j associated with excitation in the jth vibrational state. The system is subsequently photo-excited with two CW lasers with a total electric field $\bar{\varepsilon}(t)$,

$$\bar{\varepsilon}(t)=\bar{\varepsilon}_j e^{-i(\omega_j t+\theta_j)}+\bar{\varepsilon}_k e^{-i(\omega_k t+\theta_k)}+\text{c.c.}, \tag{2.3}$$

where the field amplitudes $\bar{\varepsilon}_j$ and $\bar{\varepsilon}_k$ are time independent vectors of length $|\bar{\varepsilon}_j|$, and $|\bar{\varepsilon}_k|$. The quantities θ_j and θ_k, in Eq. (2.3), are the phases of the two CW fields. If the frequencies ω_j and ω_k are chosen such that $\hbar\omega_k+E_k=\hbar\omega_j+E_j=E$, then both $|j\rangle$ and $|k\rangle$ are raised by the laser field to continuum states $|E,\xi,n^-\rangle$ of an electronic excited state with energy E. These two photoexcitation routes interfere with one another, and assuming that the field is sufficiently weak to allow the use of first order perturbation theory, the relative probability ratio $R(\xi,\xi',E)$, of producing product in arrangement channel ξ to that in arrangement ξ', at energy E, is given by[3]

$$R(\xi,\xi';E)=\frac{|\mu_{jj}(\xi,E)|+x^2|\mu_{kk}(\xi,E)|+2x\cos(\theta_j-\theta_k+\Phi_{jk}(\xi,E))|\mu_{jk}(\xi,E)|}{|\mu_{jj}(\xi',E)|+x^2|\mu_{kk}(\xi',E)|+2x\cos(\theta_j-\theta_k+\Phi_{jk}(\xi',E))|\mu_{jk}(\xi',E)|}. \tag{2.4}$$

Here, x is the ratio of controllable parameters $x=|(c_k|\bar{\varepsilon}_k|)/(c_j|\bar{\varepsilon}_j|)|$, and $\Phi_{jk}(\xi,E)$ is the phase of the cumulative transition matrix element $\mu_{jk}(\xi,E)$,

$$\mu_{j,k}(\xi,E)=|\mu_{jk}(\xi,E)|e^{i\Phi_{jk}(\xi,E)} =\langle\Psi_0(j)|\left[\sum_{n=0}^{\infty}|E,\xi,n^-\rangle\langle E,\xi,n^-|\right]|\Psi_0(k)\rangle, \tag{2.5}$$

where $|\Psi_0(j)\rangle\equiv\mu_\varepsilon|j\rangle$, and μ_ε is the dipole operator along the direction of the field. Note that the off-diagonal μ_{jk} manifest the interference between components of the continuum wave function which are excited by independent coherent excitation pathways.

Equations (2.4) and (2.5) show that the relative product yields can be experimentally controlled by changing either the composition of the initial superposition state, or the relative phase or amplitude associated with the photoexcitation laser pulses. Essentially all simulations to date have computed the cumulative transition matrix elements $\mu_{j,k}(\xi,E)$, according to Eq. (2.5), after solving first the time-independent scattering problem at the complete state-to-state level. The only exception to this has been our recent study of ICN coherent control,[22] where the photodissociation process was described in the time dependent picture, and the transition matrix elements were computed according to

$$\mu_{j,k}(\xi,E)=\lim_{t\rightarrow\infty}\sum_{n=0}^{\infty}\langle\Psi_t(j)|E,\xi,n^o\rangle\langle E,\xi,n^o|\Psi_t(k)\rangle. \tag{2.6}$$

Here $|E,\xi,n^o\rangle$ are the asymptotic states associated with photofragments that are in product channel ξ, at energy E, and internal state n. The quantities $|\Psi_t(j)\rangle$ and $|\Psi_t(k)\rangle$ result from time evolving $|\Psi_0(j)\rangle$ and $|\Psi_0(k)\rangle$ according to the excited state Hamiltonian $\hat{H}$. Hence, all methods implemented to date have required resolution into individual product states.

We wish to derive an expression that allows the determination of μ_{jk} without the need to compute dynamics into each product channel. To do so we first rewrite Eq. (2.5). The Appendix shows that the sum in brackets, in Eq. (2.5), can be written as

$$\sum_{n=0}^{\infty}|E,\xi,n^-\rangle\langle E,\xi,n^-|=\hat{P}_\xi\delta(E-\hat{H}), \tag{2.7}$$

to obtain

$$\mu_{j,k}(\xi,E)=\langle\Psi_0(j)|\hat{P}_\xi\delta(E-\hat{H})|\Psi_0(k)\rangle. \tag{2.8}$$

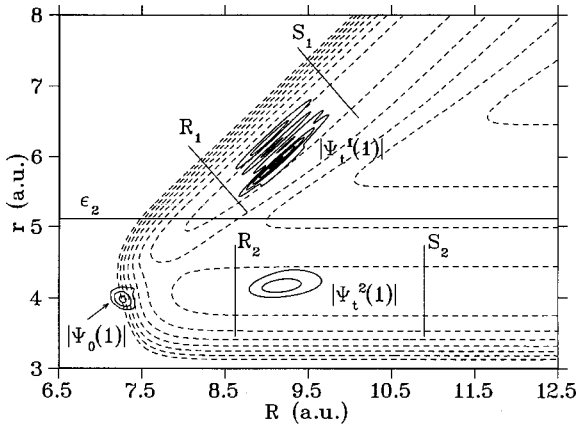

FIG. 1. Excited state potential-energy surface for unimolecular dissociation [Eq. (2.1)]. Here, $r=r_{BC}$ and $R=r_{AB}+r_{BC}m_C/(m_C+m_B)$, are the Jacobi coordinates associated with the vibrational and translational coordinates, respectively, in photofragmentation channel $\xi=2$. Shown are the dividing surfaces $R=R_1$ and $R=R_2$, the asymptotic cuts S_1 and S_2 in the free interaction regions, and the position of the absorbing potential ϵ_2 that would absorb the wave packet components $\Psi_t^1(1)$ and $\Psi_t^1(2)$ that correlate with asymptotic product channel $\xi=1$. Also shown are contour plots for the modulus of the initial wave packet, $\Psi_0(1)$, that results from photoexcitation of the ground vibrational state, and the time evolved wave packet components $\Psi_t^1(1)$ and $\Psi_t^2(1)$ at $t=40$ fs after photoexcitation of the system.

Here, $\hat{P}_\xi$ is the projection operator onto asymptotic product channel ξ, defined as

$$\hat{P}_\xi = \lim_{t\to\infty} e^{i\hat{H}t/\hbar} h_\xi(R) e^{-i\hat{H}t/\hbar}, \tag{2.9}$$

and, $h_\xi(R)$ is a function of the dissociating bond length R, associated with asymptotic channel ξ. Specifically, $h_\xi(R)$ is one on the right of the dividing surface $R=R_\xi$ and zero on the left (see Fig. 1).

Substituting Eq. (2.9) into Eq. (2.8), gives that $\mu_{j,k}(\xi,E)$ can be computed according to

$$\mu_{j,k}(\xi,E) = (2\pi\hbar)^{-1} \int_{-\infty}^{\infty} dt e^{i\omega t/\hbar} \zeta_{j,k}(\xi,t), \tag{2.10}$$

with $E=\hbar\omega$, i.e., as the Fourier transform of the survival amplitude $\zeta_{j,k}(\xi,t)$,

$$\zeta_{j,k}(\xi,t) = \langle \Psi_0^\xi(j) | \Psi_t(k) \rangle. \tag{2.11}$$

Here, $|\Psi_0^\xi(j)\rangle$ is defined according to

$$|\Psi_0^\xi(j)\rangle \equiv \hat{P}_\xi |\Psi_0(j)\rangle = \lim_{t\to\infty} e^{i\hat{H}t/\hbar} h_\xi e^{-i\hat{H}t/\hbar} |\Psi_0(j)\rangle, \tag{2.12}$$

and is the wave packet component of the initial state $|\Psi_0(j)\rangle$ that correlates with the asymptotic product channel ξ.

Semiclassical and quantum mechanical calculations, reported in Sec. V, are essentially straightforward implementations of Eq. (2.10), where the survival amplitudes $\zeta_{j,k}(\xi,t)$ are obtained according to Eqs. (2.11) and (2.12). These equations provide an efficient procedure to obtain cumulative transition matrix elements, solely in terms of survival amplitudes. These survival amplitudes are expected to decay quite rapidly during the early time relaxation process in the continuum state, since the initially interacting constituents of the system separate from one another according to alternative reaction pathways, and cease to interact thereafter.

Finally, two comments are in order. First, we note that Eq. (2.10) provides the useful computational check that

$$\sum_\xi \mathrm{Im}[\mu_{j,k}(\xi,E)] = 0, \tag{2.13}$$

when both $\Psi_0(j)$ and $\Psi_0(k)$ are real functions. Here Im[] denotes the imaginary part function of its argument. Equation (2.13) follows from noting that, according to Eq. (2.10), the sum

$$\sum_\xi \mu_{j,k}(\xi,E) = \langle \Psi_0(j) | \delta(E-\hat{H}) | \Psi_0(k) \rangle, \tag{2.14}$$

is real, since

$$\langle \Psi_0(j) | \delta(E-\hat{H}) | \Psi_0(k) \rangle = (2\pi\hbar)^{-1} 2\,\mathrm{Re}\left[\int_0^\infty dt e^{i\omega t/\hbar} \zeta_{j,k}(t) \right], \tag{2.15}$$

when $\Psi_0(j)$ and $\Psi_0(k)$ are real wave functions with $j\neq k$, and always when $j=k$. Here the survival amplitudes $\zeta_{j,k}(t)$ [Eq. (2.15)], are defined as

$$\zeta_{j,k}(t) \equiv \langle \Psi_0(j) | e^{-i\hat{H}t/\hbar} | \Psi_0(k) \rangle = \langle \Psi_0(j) | \Psi_t(k) \rangle. \tag{2.16}$$

Second, we note that the survival amplitudes $\zeta_{j,k}(\xi,t)$ could also be computed in terms of the flux through the dividing surface, $R=R_\xi$, according to the time average over motion

$$\zeta_{j,k}(\xi,t) = \langle \Psi_0(j) | h_\xi | \Psi_t(k) \rangle + \int_0^\infty dt' \langle \Psi_{t'}(j) | \hat{F}_\xi | \Psi_{t+t'}(k) \rangle, \tag{2.17}$$

where $\hat{F}_\xi$, in Eq. (2.17), is the flux operator defined as

$$\hat{F}_\xi \equiv \left(\frac{i}{\hbar} \right) [\hat{H}, h_\xi]. \tag{2.18}$$

Equation (2.17) follows from Eqs. (2.11) and (2.12), by noting that

$$\lim_{t\to\infty} e^{i\hat{H}t/\hbar} h_\xi e^{-i\hat{H}t/\hbar} = h_\xi + \frac{i}{\hbar} \int_0^\infty dt' e^{i\hat{H}t'/\hbar} (\hat{H}h_\xi - h_\xi \hat{H}) e^{-i\hat{H}t'/\hbar}. \tag{2.19}$$

A semiclassical procedure for implementing Eq. (2.17) is presented in Sec. IV B.

III. QUANTUM MECHANICAL APPROACH

The quantum mechanical procedure to compute $\mu_{jk}(E,\xi)$ in terms of Eqs. (2.10), (2.11), and (2.12), requires the propagation of each wave packet component $|\Psi_0(k)\rangle$ and $|\Psi_0(j)\rangle$ which comprise the initial superposition state. We do so in accord with the standard split-operator propagation scheme.[23]

Computations of survival amplitudes $\zeta_{j,k}(\xi,t)$ involve projections of the time evolved wave packet $|\Psi_t(k)\rangle$ onto

the initial state component $|\Psi_0^{\xi}(j)\rangle$ that correlates with asymptotic product channel ξ. To compute $|\Psi_0^{\xi}(j)\rangle$ we replace the infinite time limit, in Eq. (2.11), by a finite propagation time, τ,

$$|\Psi_0^{\xi}(j)\rangle = e^{i\hat{H}\tau/\hbar} h_{\xi} e^{-i\hat{H}\tau/\hbar} |\Psi_0(j)\rangle. \tag{3.1}$$

The quantity $|\Psi_0^{\xi}(j)\rangle$ is obtained, according to Eq. (3.1), by propagating $|\Psi_0(j)\rangle$ forward for time τ, applying h_{ξ} and then propagating the resultant wave packet backwards in time for time τ. Doing so only requires evolving the initial state $|\Psi_0(j)\rangle$ for the minimum time τ after which there is no significant overlap between the wave packet component exiting in channel ξ and the wave packet components associated with the other photofragmentation channels. Note that τ can be much shorter than the relaxation time necessary to reach the asymptotic noninteracting region.

The result of this procedure to prepare $|\Psi_0^{\xi}(j)\rangle$, is to absorb completely those wave packet components that do not correlate with the asymptotic product state ξ. This preparation of $|\Psi_0^{\xi}(j)\rangle$ can also be performed according to

$$|\Psi_0^{\xi}(j)\rangle = e^{i\hat{H}\tau/\hbar} e^{-i(\hat{H}-i\hat{\epsilon}_{\xi})\tau/\hbar} |\Psi_0(j)\rangle, \tag{3.2}$$

by performing the forward propagation in the presence of an appropriate absorbing potential, $\hat{\epsilon}_{\xi}$.[24–27] Note, that here we take advantage of the underlying simplicity of photodissociation dynamics in the continuum state, where the system cannot recross back to the interaction region after reaching a specific product region. The absorbing potential is chosen to be zero in the interaction region where the relevant dynamics for determining the survival amplitude occurs, and is ''switched on'' to absorb the product in the region of products that do not correlate with channel ξ (see Fig. 1). The finite propagation time τ, in Eq. (3.2), can then be chosen as the minimum propagation time (in the presence of the absorbing potential), necessary to absorb all wave packet components that do not correlate with the asymptotic product state ξ.

IV. SEMICLASSICAL APPROACH

Section IV A describes a semiclassical procedure to compute the cumulative transition matrix elements $\mu_{jk}(E,\xi)$ in terms of Eq. (2.10), where the survival amplitudes $\zeta_{j,k}(\xi,t)$ are obtained according to Eqs. (2.11) and (2.12). Section IV B describes a semiclassical procedure to compute the survival amplitudes $\zeta_{j,k}(\xi,t)$, according to Eq. (2.17), in terms of the flux through a dividing surface along the dissociative coordinate.

A. Absorbing boundary: Semiclassical implementation of Eqs. (2.10) and (2.11)

The semiclassical implementation of Eq. (2.10), is quite straightforward. The survival amplitudes $\zeta_{j,k}(\xi,t)$ are computed, by writing Eq. (2.12) in the form of Eq. (3.2), according to

$$\zeta_{j,k}(\xi,t) = \langle \Psi_0(j)| e^{-i\hat{H}t/\hbar} e^{i\hat{H}\tau/\hbar} e^{-i(\hat{H}-i\hat{\epsilon}_{\xi})\tau/\hbar} |\Psi_0(k)\rangle, \tag{4.1}$$

and the three time evolution operators, in Eq. (4.1), are combined into one overall SC-IVR time propagation, according to

$$\zeta_{j,k}(\xi,t) = (2\pi\hbar)^{-N} \int d\mathbf{p}_0 \int d\mathbf{q}_0 e^{i[S_t(\mathbf{p}_0,\mathbf{q}_0)+i\epsilon_{\tau}]/\hbar} \times C_t(\mathbf{p}_0,\mathbf{q}_0) \langle \Psi_0(j)|\mathbf{p}_t,\mathbf{q}_t\rangle \langle \mathbf{p}_0,\mathbf{q}_0|\Psi_0(k)\rangle, \tag{4.2}$$

where the exponential damping factor $e^{-\epsilon_{\tau}}$, arising from the absorbing potential,[28] is

$$\epsilon_{\tau} \equiv \int_0^{\tau} dt' \, \epsilon(\mathbf{q}(\mathbf{q}_0,\mathbf{p}_0;t')), \tag{4.3}$$

and can be approximated according to

$$e^{-\epsilon_{\tau}} = h_{\xi}(R_{\tau}), \tag{4.4}$$

since its only effect, in the long time limit ($\tau \to \infty$), is to eliminate the contributions of trajectories that do not dissociate into channel ξ.

Equation (4.2) is obtained by using the Herman–Kluk,[29] or coherent state IVR for the time evolution operator. The quantities $\mathbf{q}_t \equiv \mathbf{q}_t(\mathbf{p}_0,\mathbf{q}_0)$, and $\mathbf{p}_t \equiv \mathbf{p}_t(\mathbf{p}_0,\mathbf{q}_0)$, in Eq. (4.2), are the coordinates and momenta evolved for time t from the initial phase space point $(\mathbf{p}_0,\mathbf{q}_0)$, using the Hamiltonian H of the excited state. The classical action along this trajectory, $S_t(\mathbf{p}_0,\mathbf{q}_0)$, is obtained by integrating the following equation:

$$\frac{dS_t}{dt} = \mathbf{p}_t \cdot \dot{\mathbf{q}}_t - H(\mathbf{p}_t,\mathbf{q}_t), \tag{4.5}$$

along with the usual classical equations of motion,

$$\frac{dq(j)}{dt} = \frac{\partial H(\mathbf{q},\mathbf{p})}{\partial p(j)} \quad \text{and} \quad \frac{dp(j)}{dt} = -\frac{\partial H(\mathbf{q},\mathbf{p})}{\partial q(j)}. \tag{4.6}$$

The Hamiltonian $H(\mathbf{p}_t,\mathbf{q}_t)$, in Eqs. (4.5) and (4.6) above, is

$$H(\mathbf{q},\mathbf{p}) = \tfrac{1}{2}\mathbf{p}\cdot\mathbf{m}^{-1}\cdot\mathbf{p} + V(\mathbf{q}), \tag{4.7}$$

written in terms of normal mode coordinates and momenta, $\mathbf{q}$ and $\mathbf{p}$, respectively. V($\mathbf{q}$), in Eq. (4.7), is the dissociative excited state potential energy that describes the photodissociation reaction for the generic molecule ABC.

The pre-exponential factor in the integrand of Eq. (4.2) is given by

$$C_t(\mathbf{p}_0,\mathbf{q}_0) = \sqrt{\det[\mathbf{M}]}, \tag{4.8}$$

where $\mathbf{M}$ is a linear combination of components of the monodromy matrix,

$$M(j,k) = \frac{1}{2}\left(\frac{\partial q_t(k)}{\partial q_0(j)} + \frac{\gamma(j)}{\gamma(k)} \frac{\partial p_t(k)}{\partial p_0(j)} - \frac{1}{2i\hbar\gamma(k)} \frac{\partial p_t(k)}{\partial q_0(j)} - 2i\hbar\gamma(j) \frac{\partial q_t(k)}{\partial p_0(j)} \right), \tag{4.9}$$

where $\gamma(j)$ are the constant parameters in the coherent states,

$$\langle \mathbf{q}|\mathbf{q}_t,\mathbf{p}_t\rangle=\prod_{j=1}^{N}\left(\frac{2\gamma(j)}{\pi}\right)^{1/4}\exp\Big(-\gamma(j)[q(j)-q_t(j)]^2+\frac{i}{\hbar}p_t(j)[q(j)-q_t(j)]\Big), \tag{4.10}$$

and similarly for $\langle \mathbf{q}|\mathbf{q}_0,\mathbf{p}_0\rangle$.

The various time dependent partial derivatives are obtained by numerically integrating the following equations for the stability matrix

$$\frac{d}{dt}\left(\frac{\partial p_t(i)}{\partial z(j)}\right)=-\sum_{k=1}^{N}\left(\frac{\partial^2 H(\mathbf{p}_t,\mathbf{q}_t)}{\partial p_t(k)\partial q_t(i)}\frac{\partial p_t(k)}{\partial z(j)}+\frac{\partial^2 H(\mathbf{p}_t,\mathbf{q}_t)}{\partial q_t(k)\partial q_t(i)}\frac{\partial q_t(k)}{\partial z(j)}\right)$$

$$\frac{d}{dt}\left(\frac{\partial q_t(i)}{\partial z(j)}\right)=+\sum_{k=1}^{N}\left(\frac{\partial^2 H(\mathbf{p}_t,\mathbf{q}_t)}{\partial p_t(k)\partial p_t(i)}\frac{\partial p_t(k)}{\partial z(j)}+\frac{\partial^2 H(\mathbf{p}_t,\mathbf{q}_t)}{\partial q_t(k)\partial p_t(i)}\frac{\partial q_t(k)}{\partial z(j)}\right),$$

where $z=p_0$ or q_0.[30]

B. Flux evaluation: Semiclassical implementation of Eq. (2.17)

The first term on the r.h.s. of Eq. (2.17) can be computed according to the standard implementation of the SC-IVR for computations of survival amplitudes. Also, in general, this term can be neglected since the dividing surface of h_ξ can be chosen sufficiently far from the Franck–Condon region. The discussion that follows concerns practical aspects of the semiclassical implementation of Eq. (2.17) and disregards the first term on the r.h.s of Eq. (2.17).

The second term in Eq. (2.17) can also be written in the form

$$\zeta_{jk}(\xi,t')=(2\pi\hbar)^{-1}\int_0^\infty dt\langle\Psi_0(j)|\times e^{i\hat{H}t'/\hbar}\hat{F}_\xi e^{-i\hat{H}(t+t')/\hbar}|\Psi_0(k)\rangle. \tag{4.11}$$

Using the Herman–Kluk,[29] or coherent state IVR for the time evolution operator, $\zeta_{jk}(\xi,t')$ becomes a double phase space average over initial conditions for the time average over motion,

$$\zeta_{jk}(\xi,t')=(2\pi\hbar)^{-2N-1}\int d\mathbf{p}_0\int d\mathbf{q}_0\int d\mathbf{p}_0'\int d\mathbf{q}_0'\int_0^\infty dt\times e^{i(S_{t+t'}(\mathbf{p}_0,\mathbf{q}_0)-S_t(\mathbf{p}_0',\mathbf{q}_0'))/\hbar}\times C_t^*(\mathbf{p}_0',\mathbf{q}_0')C_{t+t'}(\mathbf{p}_0,\mathbf{q}_0)\times\langle\Psi_0(j)|\mathbf{p}_0',\mathbf{q}_0'\rangle\times\langle\mathbf{p}_t',\mathbf{q}_t'|\hat{F}_\xi|\mathbf{p}_{t+t'},\mathbf{q}_{t+t'}\rangle\langle\mathbf{p}_0,\mathbf{q}_0|\Psi_0(k)\rangle. \tag{4.12}$$

The integration variables $(\mathbf{p}_0,\mathbf{q}_0)$ and $(\mathbf{p}_0',\mathbf{q}_0')$, in Eq. (4.12), are the initial conditions for pairs of classical trajectories. Propagating first a trajectory that evolves according to $\mathbf{q}_{t'+t}\equiv\mathbf{q}_{t'+t}(\mathbf{p}_0,\mathbf{q}_0)$ and $\mathbf{p}_{t'+t}\equiv\mathbf{p}_{t'+t}(\mathbf{p}_0,\mathbf{q}_0)$, the time average over motion could be evaluated while one is computing the second trajectory of each pair, $\mathbf{q}_t'\equiv\mathbf{q}_t(\mathbf{p}_0',\mathbf{q}_0')$, and $\mathbf{p}'_t\equiv\mathbf{p}_t(\mathbf{p}'_0,\mathbf{q}'_0)$. Doing the t integral, in Eq. (4.12), thus would not entail any extra effort in the calculation, other than storing the time dependent quantities associated with the first trajectory. Also, the structure of Eq. (4.12) allows doing the calculation for many different values of t', i.e., all from the same set of trajectories. We have found, however, that the implementation of this method is not as efficient as the implementation procedure described in Sec. IV A, where survival amplitudes are obtained from the very early time relaxation dynamics. Hence, we utilize below the method of Sec. IV A. The direct semiclassical procedure described in this section, however, has the advantage that could be easily generalized to simulate coherent control in the presence of nonadiabatic photodissociation dynamics, as formulated in terms of the Meyer–Miller Hamiltoninan.[31,22]

V. RESULTS

Results are presented in two sections after describing the specific model Hamiltonian and the initial state in Sec. V A; Sec. V B compares the semiclassical results for survival amplitudes and transition matrix elements to the corresponding cumulative, and state-to-state resolved quantum mechanical results. Section V C then presents our semiclassical results of bichromatic coherent control, after photoexcitation of an initial superposition state to various final energy states in the continuum, and compares them to the corresponding full quantum mechanical calculations.

Semiclassical results are converged with 5×10^5 trajectories, integrated using the standard fourth-order Runge–Kutta algorithm,[32] according to the parallel programming model described in Ref. 6. Trajectories are initialized through Monte Carlo sampling of coordinates and momenta according to localized phase space distributions, determined by the coherent state transform of the initial wave packet components. This excited state population is created under the artifice that the photolysis event promotes molecules instantaneously from the ground electronic state to the optically allowed excited state that is resonant with the excitation wavelength.

A. Model Hamiltonian and initial state

The nuclear wave function that represents the initial population in the excited electronic state is assumed to be

$$\langle\mathbf{q}|\Psi_0(j)\rangle=\left(\frac{\alpha(1)\alpha(2)}{\pi^2}\right)^{1/4}H_j(\sqrt{\alpha(1)/\hbar}q(1))\times e^{(-1/2)[\alpha(1)q(1)^2-\alpha(2)q(2)^2]}, \tag{5.1}$$

where H_j is a Hermite polynomial of degree j. The coordinates $q(1)$ and $q(2)$, in Eq. (5.1), are the symmetric and antisymmetric stretching normal modes of the ABC molecule. The initial state for the control studies, introduced in Eq. (2.2), involves a linear superposition of vibrational states with $j=0$ and $j=1$. The transition dipole that couples the ground and excited electronic states is assumed to be independent of nuclear coordinates (Condon approximation).

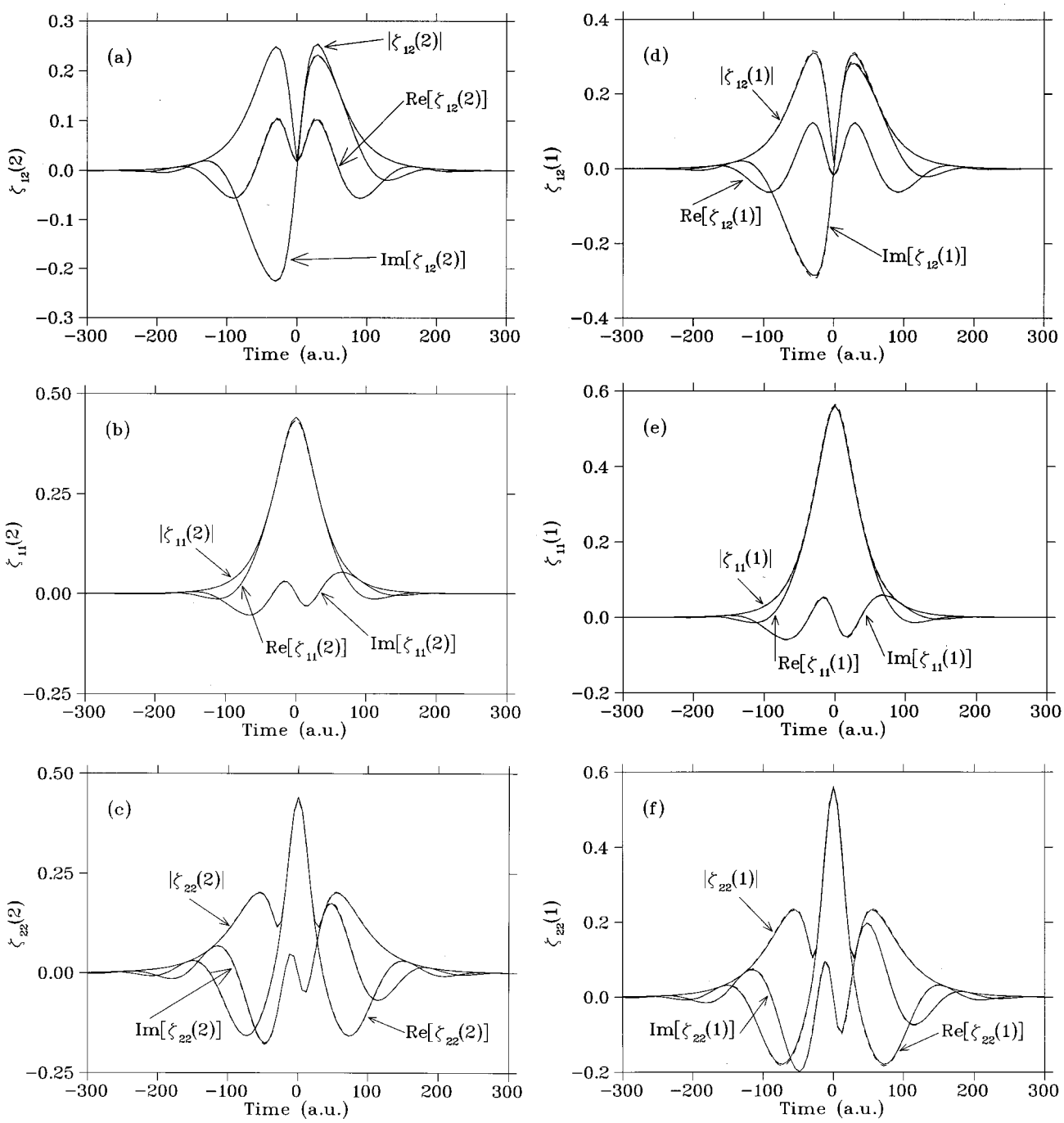

FIG. 2. Comparison of semiclassical (solid lines), and quantum mechanical results (dashes) for the modulus, real, and imaginary parts of the survival amplitudes $\zeta_{12}(\xi)$, $\zeta_{11}(\xi)$, and $\zeta_{22}(\xi)$, with $\xi=(1,2)$ as a function of time. Panels (a), (b), and (c) correspond to photodissociation channel $\xi=2$, while panels (d), (e), and (f) correspond to channel $\xi=1$.

We examine a simple collinear model for photodissociation where the ground electronic state potential energy surface is defined as a sum of two Morse potentials,

$$V_{nm}(r_{nm})=D_{nm}[e^{-\alpha_{nm}(r_{nm}-r_{nm}^{e})}-1]^2-D_{nm}, \qquad (5.2)$$

where $nm=AB$, or $nm=BC$ labels the corresponding molecular fragment. The Morse potentials are parametrized as follows: $D_{AB}=0.0874$ a.u., $\alpha_{AB}=0.87094$ a.u., $r_{AB}^{e}=4.043$ a.u., $D_{BC}=0.1069$ a.u., $\alpha_{BC}=0.9155$ a.u., $r_{BC}^{e}=3.685$ a.u. The masses for the molecular fragments A, B, and C are chosen to be those of I, CH_2, and Br, respectively. Specifically, $m_A=126.904\ m_{\mathrm{H}}$, $m_B=14.011\ m_{\mathrm{H}}$, and $m_C=79.904\ m_{\mathrm{H}}$, respectively, where m_{H} is the mass of a hydrogen atom.

The excited state potential energy surface, $V(r_{AB},r_{BC})$, is defined in terms of the internal coordinates r_{AB} and r_{BC} according to the following expression:

$$\begin{aligned}V(r_{AB},r_{BC})=&(A_{AB}e^{-\beta_{AB}r_{AB}}+V_{BC}(r_{BC}))f(x)\\&+(A_{BC}e^{-\beta_{BC}r_{BC}}+V_{AB}(r_{AB}))(1.0-f(x))\\&+D_2e^{-\alpha_2(r_{AB}-r_{AB}^{e})-\alpha_3(r_{BC}-r_{BC}^{e})}, \qquad (5.3)\end{aligned}$$

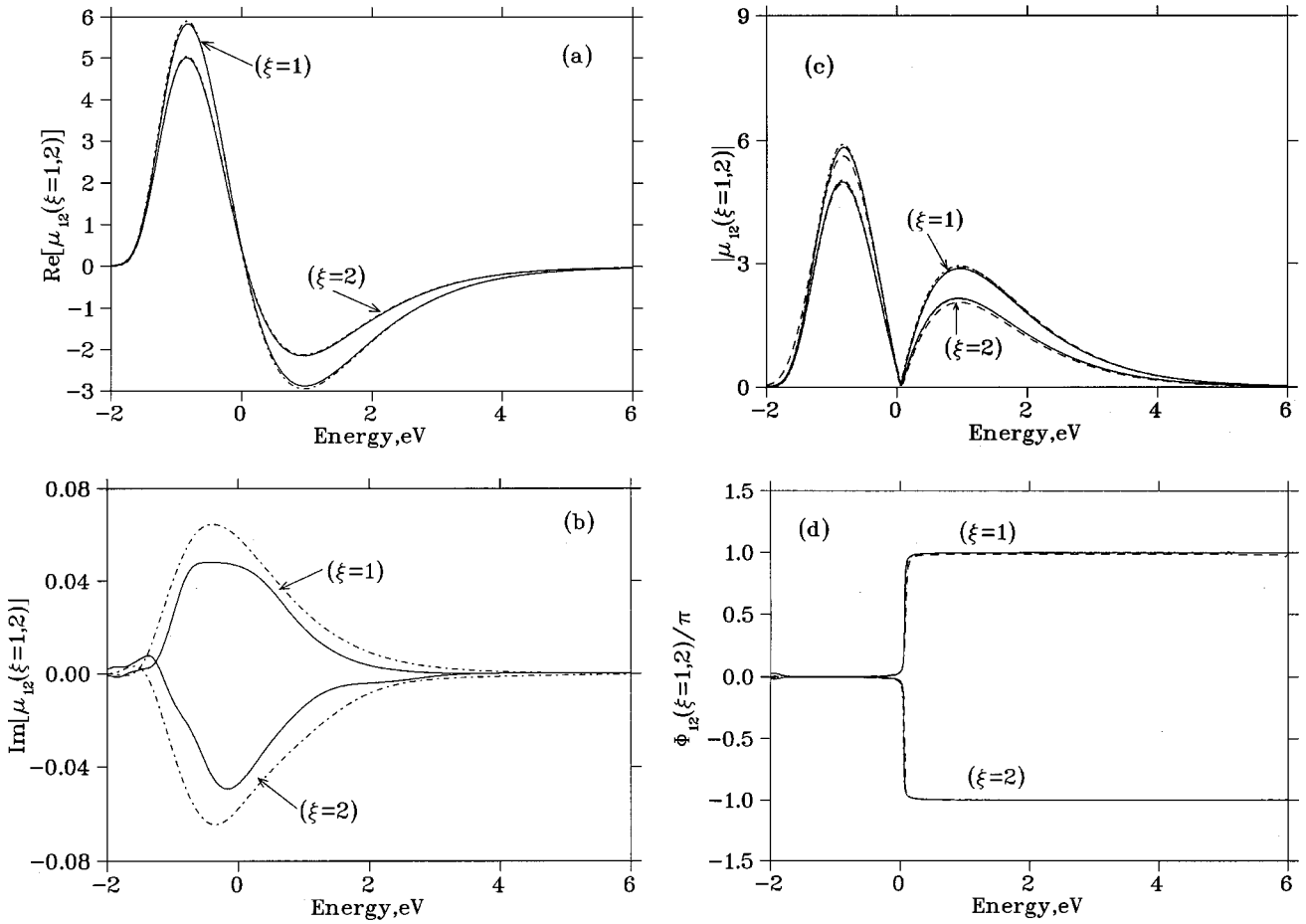

FIG. 3. Comparison of the semiclassical results (solid lines) for the cumulative transition matrix elements $\mu_{12}(\xi=1,2)$, as a function of the total energy E in the continuum state, to state-resolved (dashes) and cumulative (broken dashes) quantum mechanical calculations. Panels (a) and (b) show the real and imaginary parts of $\mu_{12}(\xi=1,2)$, respectively. Note the difference in scale of the ordinate of panel (b). Panel (c) shows the modulus $|\mu_{12}(\xi=1,2)|$, and panel (d) the phases Φ_{12}, as a function of final energy E in the continuum.

where $V_{BC}(r_{BC})$ and $V_{AB}(r_{AB})$ are the Morse potentials, introduced by Eq. (5.2), that parametrize the ground electronic state; $A_{AB}=0.37$, $\beta_{AB}=1.5$, $\alpha_2=4.8$, $\alpha_3=4.8$, $D_2=0.08824$. The function $f(x)$, in Eq. (5.3), is defined according to

$$f(x)=1/(1+e^{\alpha_h(x-x_h)}), \quad \text{with} \quad x=r_{BC}/(r_{AB}+r_{BC}), \tag{5.4}$$

where, $\alpha_h=90$, and $x_h=0.44643$.[33]

All forces and second derivatives necessary for integrating the equations of motion are calculated using finite difference expressions. Full quantum mechanical results are obtained using the fast Fourier transform (FFT) method with an extended grid of 1024 points in both the r and R Jacobi coordinates, defined in the range of coordinates $|R-9.5 \text{ a.u.}|<3$ a.u. and $|r-6 \text{ a.u}|<3$ a.u.

B. Survival amplitudes and transition matrix elements

Figure 2 compares the semiclassical results (solid lines), with the corresponding full quantum mechanical results (dashes) for the modulus, real, and imaginary parts of survival amplitudes $\zeta_{12}(\xi)$, $\zeta_{11}(\xi)$, and $\zeta_{22}(\xi)$, with $\xi=(1,2)$, as a function of time. Panels (a), (b), and (c) correspond to photodissociation channel $\xi=2$, while panels (d), (e), and (f) show the corresponding quantities for channel $\xi=1$. The comparison shows that the semiclassical survival amplitudes are in excellent agreement with quantum mechanical results; so good, in fact, that the dashed and solid lines often overlap. Figure 2 shows that both the diagonal and off-diagonal survival amplitudes decay for this particular model system within 7 fs ($\sim$290 a.u.). This relaxation time is significantly shorter than the time necessary to reach the asymptotic noninteracting region at $\sim$40 fs after photoexcitation of the system. Figure 2 also shows a significant difference between the diagonal and the off-diagonal survival amplitudes; while $\zeta_{11}(\xi=1,2)$ and $\zeta_{11}(\xi=1,2)$ are symmetric relative to $t=0$, and satisfy the condition that $\zeta_{jj}(\xi,t)=\zeta_{jj}^*(\xi,-t)$, the off-diagonal survival amplitudes $\zeta_{jk}(\xi=1,2)$ are slightly asymmetric relative to $t=0$. For example, note that the maximum of $|\zeta_{jk}(\xi=1,2)|$ at positive times is slightly higher than the maximum at negative times. This asymmetry results from an asymmetric potential energy surface, and makes its Fourier transform μ_{12} a complex quantity with nonzero real and imaginary parts.

Figure 3 shows the comparison of semiclassical (solid lines), and quantum mechanical (dashes) results for the real [panel (a)] and imaginary [panel (b)] parts of $\mu_{12}(\xi=1,2)$.

Figure 3, also compares of the modulus $|\mu_{12}(\xi=1,2)|$ [see panel (c)], and phase $\Phi_{12}(\xi=1,2)$ [panel (d)] of the cumulative transition matrix elements $\mu_{12}(\xi=1,2)$, as a function of the total energy E in the continuum state, obtained according to the semiclassical method (solid lines), the quantum state-resolved (dashes) approach, and quantum cumulative (broken dashes) methodology. Although one can see small differences, both the modulus and the phase of the cumulative transition matrix elements obtained semiclassically are in very good agreement with full quantum mechanical simulations over the whole energy range. The semiclassical results are able to reproduce the correct shape of $|\mu_{12}(\xi=1,2)|$, and the position of the amplitude nodes as a function of E, as well as the energy dependence of the phase $\Phi_{12}(\xi=1,2)|$, that is found to be in almost quantitative agreement with full quantum mechanical calculations in both photofragmentation channels. Figure 3 shows that the most important features of $\mu_{12}(\xi=1,2)$ include the energy position of the node, the quality of the node (the amplitude does not totally vanish at the node), and the change in sign of $\mu_{12}(\xi=1,2)$ when going through the energy node ($\Delta\Phi_{12}=+/-\pi$). These features can be understood in terms of the symmetry properties of the product of the two wave packet components that contribute to $\mu_{12}(\xi=1,2)$ at each n, as defined by Eq. (2.6). The comparison of real and imaginary parts shows more clearly the level of agreement between the quantum and semiclassical results for a model system where the imaginary parts of $\mu_{12}(\xi=1,2)$ are much smaller than the real parts throughout the whole energy range.

Figure 4 compares the semiclassical results (solid lines) for the diagonal cumulative matrix elements $\mu_{11}(\xi=1,2)$ [see panel (a)], and $\mu_{22}(\xi=1,2)$ [see panel (b)], with the corresponding state-resolved [dashes], and cumulative (broken dashes) quantum mechanical results. One sees that with the exception of small deviations there is almost quantitative agreement between semiclassical and full quantum mechanical calculations of the cumulative transition amplitudes associated with ground and excited vibrational states, for both photodissociation channels.

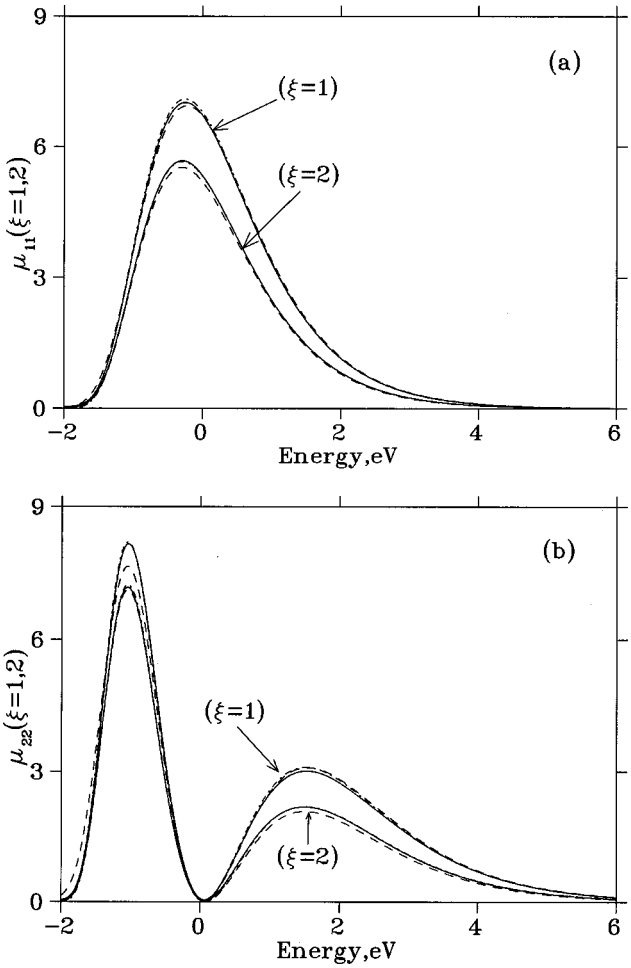

FIG. 4. Comparison between the semiclassical results (solid lines) for the cumulative matrix elements $\mu_{11}(\xi)$ and $\mu_{22}(\xi)$, with $\xi=(1,2)$, and the corresponding state-resolved (dashes) and cumulative (broken lines) quantum mechanical results. Panel (a) shows the comparison of $\mu_{11}(\xi=1,2)$, and panel (b) displays the corresponding results for $\mu_{22}(\xi=1,2)$.

C. Coherent control of photofragmentation product yields

Figure 5 shows the percentage product yields $100\times A/(A+C)$, obtained from Eq. (2.4), after photodissociation in the continuum. Bichromatic coherent control is simulated for an initial superposition of vibrational states with quantum numbers $\nu=1$ and $\nu=2$, respectively. Figure 5 compares the SC (solid lines) and full quantum mechanical (dashed lines) results obtained at various photoexcitation energies. Percentage product yields are presented in the form of contour plots for the photoexcitation energies indicated in panels (a)–(f), as a function of both the relative pulse phase parameter, $\Theta_1-\Theta_2$, and the relative amplitude $S=(c_1^2\overline{\varepsilon_1^2}/(c_2^2\overline{\varepsilon_2^2}+c_1^2\overline{\varepsilon_1^2})$.

Figure 5 shows that the model system considered herein is particularly challenging, since the relative product yields change only moderately as a function of the relative phase parameter. However, the overall comparison between SC and full quantum dynamics simulations of coherent control, indicates that the structure of the diagrams, the trend in these structures with photoexcitation energy, and the range of quantum mechanical product yields, are reproduced by the semiclassical calculations within an error of approximately 1%–5%.

At the lowest photoexcitation energy [see panel (a)], there is maximum control at $S\leqslant 0.5$, where the production of A can be reduced from 50% to 40%, by changing the relative phase parameter from 0° to 180°. At higher values of S (when $S\rightarrow 1$), the semiclassical and full quantum mechanical product yields still agree with one another within an error of 1%–5%, and show a qualitatively different behavior from that observed at smaller values of S. The major difference to note is that the degree of yield control becomes only weakly dependent on the relative phase parameter, $\Theta_1-\Theta_2$ at larger S, and is therefore no longer possible to control the final outcome of the chemical reaction via interference effects.

At higher photoexcitation energies [panel (b)] the SC and full quantum mechanical product yields again agree within about 1%–5% error and show a diagram structure as

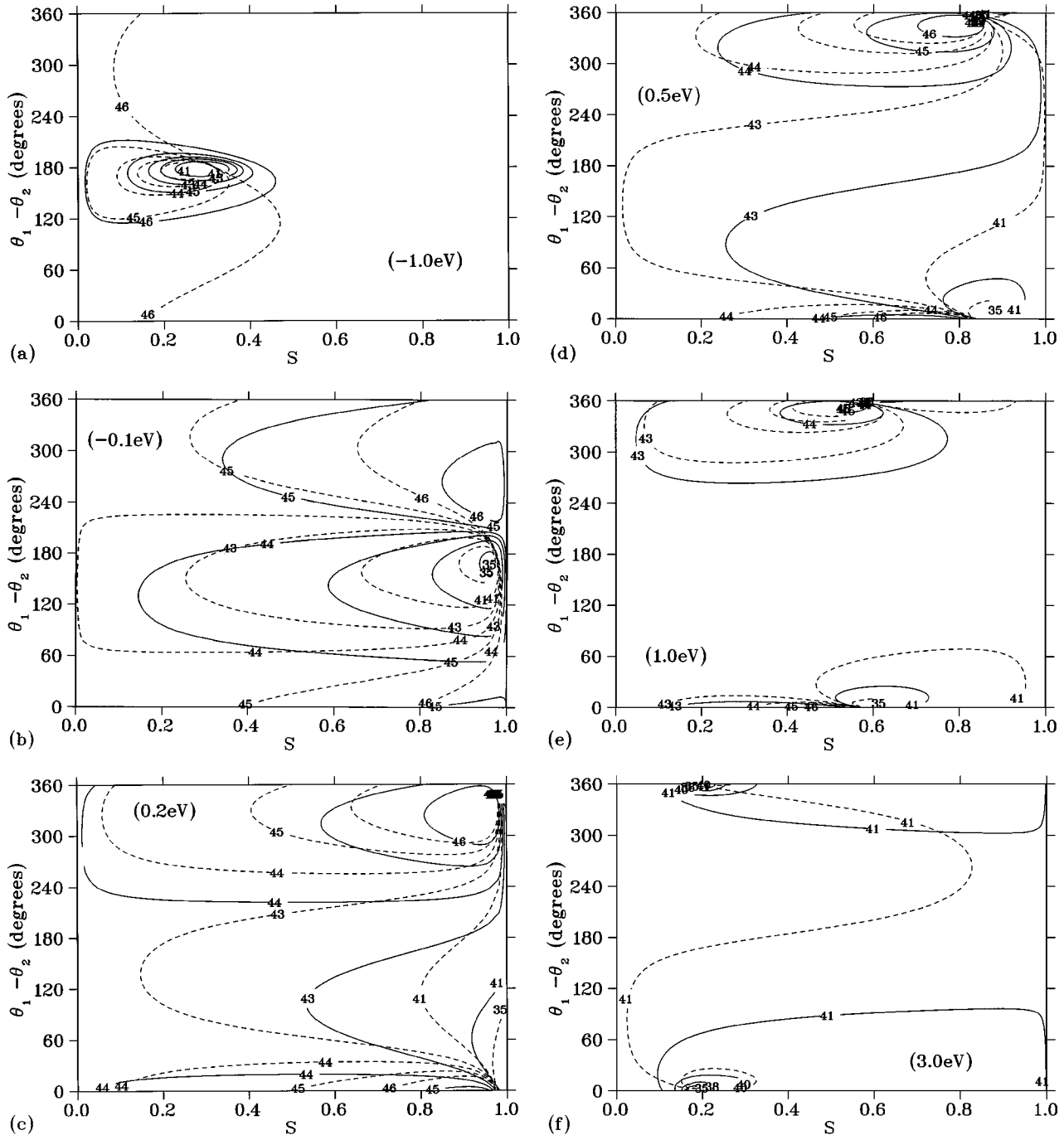

FIG. 5. Contour plots of the relative product yields $100 \times A/(A+C)$, for bichromatic coherent control of an initial ABC superposition state with symmetric stretch vibrational quantum numbers $\nu=1$ and $\nu=2$, respectively. The photoexcitation energy is indicated in each panel, relative to the energy of the isolated fragments.

a function of controllable parameters that is completely different from the diagram obtained at lower photoexcitation energies. The degree of yield control is found to be maximum in the $0.9 \leqslant S \leqslant 1.0$ range, where the production of A can be reduced from more than 45% to less than 35% by changing the relative phases from about 0° to 180°.

At even higher photoexcitation energies [panel (c)] the contour diagram is once again totally different from the diagrams obtained at lower photoexcitation energies, however, the SC and full quantum mechanical calculations agree in predicting that a maximum degree of yield control can be achieved in the $0.9 \leqslant S \leqslant 1.0$ range. Within this range of relative amplitude parameter the production of A is less than 38%, at approximately 30°, and can be increased to more than 45%, by changing the relative phases to the 280°–300° range.

Coherent control vanishes when the final energy is > 3.0 eV [panel (f)]. Panel (f) shows than SC and full quantum calculations agree in predicting that there is practically no coherent control at this particular final energy, in terms of contour lines of percentage yields that agree within 1%–5% error.

Finally, at intermediate photoexcitation energies [panels (d) and (e)], SC and full quantum mechanical calculations agree once again with one another within the same error range and predict that moderate coherence control is recovered.

VI. CONCLUSIONS

In this article we have derived formally exact quantum mechanical expressions for cumulative transition matrix elements, and we have shown that these expressions provide a useful means for simulating one photon control scenarios, such as bichromatic control of an initial superposition state, without having to solve the complete state-to-state quantum mechanical reactive scattering problem.

We have shown how to implement these exact quantum mechanical expressions both quantum mechanically, and semiclassically by using an initial value representation method, in order to investigate quantum control in a generic reaction that describes unimolecular decomposition into more than one possible product.

We have demonstrated the capabilities of the semiclassical approach by comparing the semiclassical results to full quantum mechanical calculations of photofragmentation product yields, as controlled by the relative pulse phase, and the relative amplitude parameters. We have shown that semiclassical results, obtained through quantization of the classical Hamiltonian, according to the Herman–Kluk SC-IVR methodology, together with stationary phase MC methods, were able to reproduce the correct structure of the relative product yield diagrams for various different photoexcitation energies. These results demonstrate that the cumulative SC-IVR methodology, developed in this paper, is an efficient and reliable approach to describe laser induced quantum interferences between alternative photodissociation pathways.

According to the present implementation, semiclassical simulations of coherent control require only the evaluation of survival amplitudes. The SC-IVR has already been successfully implemented for computing survival amplitudes, associated with diagonal transition matrix elements, for systems of up to 35 coupled degrees of freedom.[10] Therefore, one expects that the computational method developed in this paper should be a tractable and reliable approach for simulating coherent control in systems of high dimensionality. Such work is in progress.[34]

ACKNOWLEDGMENTS

We gratefully acknowledge financial support for this work from Photonics Research Ontario and from the U.S. Office of Naval Research. We also acknowledge a generous allocation of supercomputing time from the National Energy Research Scientific Computing Center (NERSC).

APPENDIX: DERIVATION OF EQ. (3.6)

In this Appendix we show that

$$\hat{P}_{E,\xi} \equiv \sum_{n=0}^{\infty} |E,\xi,n^-\rangle\langle E,\xi,n^-| = \hat{P}_{\xi}\delta(E-\hat{H}), \tag{A1}$$

where the spatial projection operator $\hat{P}_{\xi}$ is defined as

$$\hat{P}_{\xi} = \lim_{t\to\infty} e^{i\hat{H}t/\hbar} h_{\xi}(R) e^{-i\hat{H}t/\hbar}. \tag{A2}$$

Here, $h_{\xi}(R)$ is a function of the dissociating bond length R associated with asymptotic channel ξ. The function $h_{\xi}(R)$ is defined as 1(0) on the right(left) of a dividing surface $R = R_{\xi}$. The scattering states $|E,\xi,n^-\rangle$, in Eq. (A1), satisfy the Schrödinger equation,

$$(\hat{H}-E)|E,\xi,n^-\rangle = 0, \tag{A3}$$

and are normalized according to

$$\langle E',\xi',n'^-|E,\xi,n^-\rangle = \delta(E-E')\,\delta_{\xi,\xi'}\,\delta_{n,n'}. \tag{A4}$$

First, we insert the delta function $\delta(\hat{H}-E)$, into Eq. (A1), according to

$$\hat{P}_{E,\xi} = \sum_{n=0}^{\infty} \int_{-\infty}^{\infty} dE'\,\delta(\hat{H}-E)|E',\xi,n^-\rangle\langle E',\xi,n^-|, \tag{A5}$$

and then we evoke time-dependent scattering theory[35] to express the scattering states $|E,\xi,n^-\rangle$ in terms of the asymptotic free states $|E,\xi,n^o\rangle$,

$$|E,\xi,n^-\rangle = \lim_{t\to\infty} e^{i(\hat{H}-E)t/\hbar}|E,\xi,n^o\rangle. \tag{A6}$$

Substituting Eq. (A6) into Eq. (A5) we obtain

$$\hat{P}_{E,\xi} = \lim_{t\to\infty} e^{i\hat{H}t/\hbar}\,\delta(\hat{H}-E) \times\left[\sum_{n=0}^{\infty}\int_{-\infty}^{\infty} dE'|E',\xi,n^o\rangle\langle E',\xi,n^o|\right] e^{-i\hat{H}t/\hbar}. \tag{A7}$$

Here, $|E',\xi,n^o\rangle$ are free states of photofragments that evolve according to the free Hamiltonian in the ξ channel,

$$\hat{H}^o \equiv \lim_{R\to\infty} \hat{H} = \frac{K^2}{2\mu} + \epsilon_n, \tag{A8}$$

in the recoil direction of *positive* momenta K (conjugate to the jacobi coordinate R), energy E', and internal quantum states n of energy ϵ_n.

Hence, we can change integration variables, in Eq. (A7), to obtain

$$\hat{P}_{E,\xi} = \lim_{t\to\infty} e^{i\hat{H}t/\hbar}\,\delta(\hat{H}-E) \times\left[\sum_{n=0}^{\infty}\int_{0}^{\infty} dK|K,n^o\rangle\langle K,n^o|\right] e^{-i\hat{H}t/\hbar}, \tag{A9}$$

where the free states $|K,n^o\rangle$, introduced by Eq. (A9), are normalized according to

$$\langle K',n'^o|K,n^o\rangle = \delta(K-K')\,\delta_{n,n'}. \tag{A10}$$

Equation (A9) involves the sum over a complete set in the space of the vibrational coordinate. However, the translational scattering wavefunctions are not complete, since they cover only the range of positive momenta. In order to com-

plete the integration range in Eq. (A9), we introduce the step function $h_\xi(K)$, defined as 1(0) for positive(negative) values of its argument, and obtain

$$\hat{P}_{E,\xi} = \lim_{t\to\infty} e^{i\hat{H}t/\hbar}\delta(\hat{H}-E) \times\left[\sum_{n=0}^{\infty}\int_{-\infty}^{\infty} dK h_\xi(K)|K,n^o\rangle\langle K,n^o|\right] e^{-i\hat{H}t/\hbar}. \tag{A11}$$

After substituting the closure,

$$\hat{1} = \sum_{n=0}^{\infty}\int_{-\infty}^{\infty} dK|K,n^o\rangle\langle K,n^o|, \tag{A12}$$

we can rewrite Eq. (A11) in terms of the translation momentum operator $\hat{K}$,

$$\hat{P}_{E,\xi} = \lim_{t\to\infty} \delta(\hat{H}-E)e^{i\hat{H}t/\hbar}h_\xi(\hat{K})e^{-i\hat{H}t/\hbar}. \tag{A13}$$

Equation (A1) can be directly obtained from Eq. (A13), by replacing the momentum projection operator,

$$\hat{P}_\xi = \lim_{t\to\infty} e^{i\hat{H}t/\hbar}h_\xi(\hat{K})e^{-i\hat{H}t/\hbar}, \tag{A14}$$

by the spatial projection operator introduced in Eq. (A2). These two projection operators are equivalent, as explicitly shown in Appendix A of Ref. 36.

Finally, we note that Eq. (A13) can also be written in the symmetric form,

$$\hat{P}_{E,\xi} = \hat{P}_\xi\delta(\hat{H}-E)\hat{P}_\xi = \lim_{t\to\infty} e^{i\hat{H}t/\hbar}h_\xi\delta(\hat{H}-E)h_\xi e^{-i\hat{H}t/\hbar}, \tag{A15}$$

noting that $\hat{P}_\xi^2 = \hat{P}_\xi$, and that $\hat{P}_\xi$ and $\delta(\hat{H}-E)$ commute.

Comment: The procedure described in Sec. IV A, is more efficient than a more standard ''forward-backward'' approach, such as

$$\zeta_{j,k}(\xi,t) = (2\pi\hbar)^{-N}\int_{-\infty}^{\infty} dp_s(2\pi i p_s)^{-1}\int d\mathbf{p}_0\int d\mathbf{q}_0 \times e^{iS_t(\mathbf{p}_0,\mathbf{q}_0)/\hbar}C_t(\mathbf{p}_0,\mathbf{q}_0)\times\langle\Psi_0(j)|\mathbf{p}_t,\mathbf{q}_t\rangle \times\langle\mathbf{p}_0,\mathbf{q}_0|\Psi_0(k)\rangle, \tag{A16}$$

where the partial contribution of a single trajectory would require forward propagation from the initial phase point $(\mathbf{p}_0,\mathbf{q}_0)$ to the resulting phase point $(\mathbf{p}_\tau,\mathbf{q}_\tau)$ at time τ, then a ''momentum jump'' at time τ,

$$\mathbf{p}'_\tau = \mathbf{p}_\tau + p_s\left[\frac{\partial s(\mathbf{q})}{\partial\mathbf{q}}\right]_{\mathbf{q}=\mathbf{q}_\tau}, \tag{A17}$$

then backward propagation from the phase point $(\mathbf{p}'_\tau,\mathbf{q}_\tau)$ to phase point $(\mathbf{p}'_0,\mathbf{q}'_0)$, and finally propagation for time t, from phase point $(\mathbf{p}'_0,\mathbf{q}'_0)$ to phase point $(\mathbf{p}_t,\mathbf{q}_t)$ (see Ref. 31). Note that in contrast to Eq. (4.2), the integrand in Eq. (A16) does not include any damping factor. Therefore, according to Eq. (A16), all contributions of trajectories that do not photodissociate into channel ξ would have to be cancelled out through destructive interference.

[1] M. Shapiro and P. Brumer, in *Adv. in Atom., Mol. and Opt. Phys.*, edited by B. Bederson and H. Walther (Academic, San Diego, 2000), pp. 287–343.
[2] S. A. Rice and M. Zhao, in *Optical Control of Molecular Dynamics* (Wiley, New York, 2000).
[3] P. Brumer and M. Shapiro, Chem. Phys. Lett. **126**, 541 (1986).
[4] T. Seodeman, M. Shapiro, and P. Brumer, J. Chem. Phys. **90**, 7132 (1989).
[5] W. H. Miller, J. Chem. Phys. **53**, 3578 (1970).
[6] V. S. Batista and W. H. Miller, J. Chem. Phys. **108**, 498 (1998).
[7] V. S. Batista, M. T. Zanni, B. T. Greenblatt, D. M. Neumark, and W. H. Miller, J. Chem. Phys. **110**, 3736 (1999).
[8] V. Guallar, V. S. Batista, and W. H. Miller, J. Chem. Phys. **110**, 9922 (1999).
[9] E. A. Coronado, V. S. Batista, and W. H. Miller, J. Chem. Phys. **112**, 5566 (2000).
[10] V. Guallar, V. S. Batista, and W. H. Miller, J. Chem. Phys. **113**, 9510 (2000).
[11] G. Campolieti and P. Brumer, Phys. Rev. A **50**, 997 (1994).
[12] K. G. Kay, J. Chem. Phys. **100**, 4432 (1994).
[13] K. G. Kay, J. Chem. Phys. **101**, 2250 (1994).
[14] M. L. Brewer, J. S. Hulme, and D. E. Manolopoulos, J. Chem. Phys. **106**, 4832 (1997).
[15] B. E. Guerin and M. F. Herman, Chem. Phys. Lett. **286**, 361 (1998).
[16] E. J. Heller, J. Chem. Phys. **95**, 9431 (1991).
[17] F. Grossmann and E. J. Heller, Chem. Phys. Lett. **241**, 45 (1995).
[18] S. Garashchuk, F. Grossmann, and D. J. Tannor, J. Chem. Soc., Faraday Trans. **93**, 781 (1997).
[19] D. V. Shalashilin and B. Jackson, Chem. Phys. Lett. **291**, 143 (1998).
[20] D. Provost and P. Brumer, Phys. Rev. Lett. **74**, 250 (1995).
[21] X. Sun and W. H. Miller, J. Chem. Phys. **110**, 6635 (1999).
[22] V. S. Batista and P. Brumer, J. Phys. Chem. A **105**, 2591 (2001).
[23] J. A. Fleck, Jr., J. R. Morris, and M. D. Feit, Appl. Phys. **10**, 129 (1976).
[24] A. Goldberg and B. W. Shore, J. Phys. B **11**, 3339 (1978).
[25] C. Leforestier and R. Wyatt, J. Chem. Phys. **78**, 2334 (1983).
[26] R. Kosloff and D. Kosloff, J. Comput. Phys. **63**, 363 (1986).
[27] D. Neuhauser and M. Baer, J. Chem. Phys. **90**, 4351 (1989).
[28] B. Spath and W. H. Miller, J. Chem. Phys. **104**, 95 (1996).
[29] M. F. Herman and E. Kluk, Chem. Phys. **91**, 27 (1984).
[30] See Eqs. (A16) and (A17) in the Appendix.
[31] X. Sun and W. H. Miller, J. Chem. Phys. **106**, 6346 (1997).
[32] W. H. Press, B. P. Flannery, S. A. Teukolsky, and W. T. Vetterling, in *Numerical Recipes* (Cambridge University Press, Cambridge, 1986).
[33] This potential, however, is not designed to model true CH_2IBr photodissociation. For the latter, see D. Abrashkevich and P. Brumer (to be published).
[34] V. S. Batista and P. Brumer, J. Phys. Chem. (to be submitted).
[35] R. G. Newton, in *Scattering Theory of Waves and Particles* (McGraw–Hill, New York, 1966).
[36] W. H. Miller, S. D. Schwartz, and J. W. Tromp, J. Chem. Phys. **79**, 4889 (1983).